HHS Public Access

Author manuscript

Nature. Author manuscript; available in PMC 2015 November 28.

Published in final edited form as:

Nature. 2015 May 28; 521(7553): 516–519. doi:10.1038/nature14485.

Counteraction of antibiotic production and degradation stabilizes microbial communities

Eric D. Kelsic[1], **Jeffrey Zhao**[1], **Kalin Vetsigian**[*,2], and **Roy Kishony**[*,1,3]

[1] Department of Systems Biology, Harvard Medical School, Boston, Massachusetts, USA

[2] Department of Bacteriology and Wisconsin Institute for Discovery, University of Wisconsin-Madison, Madison, Wisconsin, USA

[3] Faculty of Biology and Department of Computer Science, Technion-Israel Institute of Technology, Haifa, Israel

Summary

A major challenge in theoretical ecology is understanding how natural microbial communities support species diversity[1-8], and in particular how antibiotic producing, sensitive and resistant species coexist[9-15]. While cyclic "rock-paper-scissors" interactions can stabilize communities in spatial environments[9-11], coexistence in unstructured environments remains an enigma[12,16]. Here, using simulations and analytical models, we show that the opposing actions of antibiotic production and degradation enable coexistence even in well-mixed environments. Coexistence depends on 3-way interactions where an antibiotic degrading species attenuates the inhibitory interactions between two other species. These 3-way interactions enable coexistence that is robust to substantial differences in inherent species growth rates and to invasion by "cheating" species that cease producing or degrading antibiotics. At least two antibiotics are required for stability, with greater numbers of antibiotics enabling more complex communities and diverse dynamical behaviors ranging from stable fixed-points to limit cycles and chaos. Together, these results show how multi-species antibiotic interactions can generate ecological stability in both spatial and mixed microbial communities, suggesting strategies for engineering synthetic ecosystems and highlighting the importance of toxin production and degradation for microbial biodiversity.

Antibiotic producing species are common in natural microbial communities[13,17,18]. Ecological models of antibiotics typically assume pairwise species relationships, where antibiotic producers inhibit sensitive species more than resistant species. These pairwise inhibitory interactions, combined with costs for production and resistance, can lead to relationships of cyclic dominance among species (e.g. "rock-paper-scissors" games), which can support coexistence in spatial environments[9-11] beyond the limit set by competitive

*Correspondence and requests for materials should be addressed to KV (kalin@discovery.wisc.edu) and RK (rkishony@technion.ac.il).

Author Contributions: EDK, KV, RK designed the study; EDK, KV, JZ did the experiments; EDK, KV did the simulations and modeling; EDK, KV, RK analyzed the data and wrote the paper.

The authors declare no competing financial interests.

exclusion[4,5]. However, such pairwise interaction models lead to coexistence through the separation of species into distinct spatial domains, whereas in nature antibiotic producing, resistant and sensitive species appear to intermix even at very small length scales[17,19]. Furthermore, species communities stabilized through pairwise antibiotic interactions are not resilient to the high level of species dispersal expected in nature[12,16]. Understanding how multiple antibiotic producing species coexist despite dispersal remains an open question.

The inhibitory interaction between an antibiotic producing species and an antibiotic sensitive species can be attenuated by the presence of a third "modulator" species (Fig. 1a). One established mechanism for antibiotic attenuation is enzymatic degradation[20], a common mechanism for antibiotic resistance[21]. In principle, a modulator species could also intensify inhibitory interactions between two species[22,23], for example by inducing antibiotic production. However, when testing for such interactions among a collection of soil isolates using a 3-species interaction assay (Fig. 1b), we observed that intensification was rare while attenuation was common (Extended Data Fig. 1-2; Extended Data Table 1). Realizing that such 3-way attenuating interactions commonly occur among natural species motivated us to explore their impact on ecological dynamics. We focus on antibiotic attenuation caused by degradation, which we observed experimentally (Extended Data Fig. 1d, Extended Data Fig. 2c), but our analysis can be generalized to other attenuation mechanisms such as antibiotic suppression[24]. It is known that antibiotic degrading species can coexist together with sensitive species when an antibiotic is provided externally[25-27]. However, when antibiotics are produced by the species themselves, these two-species communities are no longer stabilized by degradation[27,28]. The impact of antibiotic degrading species on the stability of larger ecosystems has not been explored.

We investigated how antibiotic degrading species affect the dynamics of microbial communities containing antibiotic producers by modifying a classical spatial model of antibiotic mediated interactions. As in previous spatial models of antibiotic inhibition[9-12], we consider antibiotic producing (P), sensitive (S) or resistant (R) species phenotypes. However, unlike in previous models, in addition to intrinsic resistance (R_I) we also consider resistance through antibiotic degradation (R_D) (Fig. 1ab). Antibiotic degrading species remove antibiotics from nearby locations, thereby protecting not only themselves but also neighboring species. The simulations are performed on a grid (Fig. 1c), with each simulation step consisting of: production of antibiotics around P species (within area of size K_P), removal of antibiotics near R_D species (within area of size K_D), killing of S species within the antibiotic zones, and finally colonization of empty regions on a new grid by randomly choosing surviving species within a given dispersal radius, $r_{dispersal}$ (Extended Data Fig. 3, Methods).

In these spatial inhibition-zone models, communities with intrinsic resistance and with resistance through antibiotic degradation result in dramatically different patterning and robustness to dispersal. We simulated a simple 3-species and 3-antibiotic network that exhibits cyclic dominance. Consistent with previous studies[9-12], pairwise interactions among intrinsically resistant species result in coexistence of all three species through single-species domains that continually chase each other around the grid (Fig. 1d, left). However, we found that 3-way interactions created by antibiotic degradation lead to tight intermixing of species

(Fig. 1d, right). This fine-scale intermixing let us ask whether a spatial environment was at all necessary for the coexistence of these antibiotic degrading communities. Spatial structure is needed for coexistence in pairwise antibiotic interaction models[9-12], and indeed diversity of the community with intrinsic resistance collapses when the dispersal radius increases (Fig. 1e, left; Supplementary Videos 1-5). In contrast, the antibiotic degrading community maintains diversity across any level of dispersal, even with complete mixing between time steps (Fig. 1e, right; Supplementary Videos 6-10).

We characterized the stability of these communities with respect to model parameters by considering the analytical limit of an infinitely large environment with complete mixing between time steps ($r_{dispersal} \to \infty$; a "mixed inhibition-zone model", Methods). Considering different initial species abundances, the community with intrinsically resistant species coexists only at a single unstable fixed point; starting in any other initial condition leads to extinction of all but one species (Fig. 2a, left). In striking contrast, the community with antibiotic degradation coexists with a stable fixed point and a large basin of attraction (Fig. 2a, right). Moreover, antibiotic degradation enables stable communities to form despite large differences in inherent species growth rates (g_1, g_2, g_3; Fig. 2b, right). Thus, even in environments with complete mixing, the interplay of antibiotic production and degradation leads to coexistence that is robust to large perturbations of species abundances and substantial differences in inherent growth rates.

Community stability is maximized at intermediate levels of antibiotic degradation (Fig. 2c, Extended Data Fig. 4a). Levels of degradation that are too high mostly eliminate the effects of the antibiotics, after which inherent growth rate differences lead to one species taking over. Levels of degradation that are too low do not allow coexistence, as expected, since $K_D=0$ is equivalent to intrinsic antibiotic resistance. Stability is therefore maximal at intermediate levels of degradation where a negative feedback can operate, such that increased abundance of a given species results in its increased inhibition (Extended Data Fig. 4b-d). In contrast, stability is maximal at high levels of antibiotic production (K_P). Thus, strong antibiotic production can stabilize diversity when combined with intermediate levels of antibiotic degradation.

Production and degradation of multiple antibiotics also leads to robust coexistence in a well-mixed chemostat setting. We modeled the cyclic 3-species 3-antibiotic interaction network using a single resource chemostat model. While these models are inherently unstable with intrinsic resistance, implementing resistance through enzymatic degradation of antibiotics allows coexistence of all species through stable fixed points or limit cycles (Methods). As in the inhibition-zone model, stability occurs despite inherent growth rate differences among species and was strengthened at high levels of production (K_P) and intermediate levels of degradation (K_D) (Extended Data Fig. 5a). We also observed robust coexistence for different forms of antibiotic inhibition functions and when inhibitory interactions are diffuse[29], i.e. when all species have finite sensitivity to each antibiotic (Extended Data Fig. 5b). This generality with respect to different models, assumptions, and parameter values suggests that the counteraction of antibiotic production and degradation can support coexistence in a wide variety of settings.

These 3-species ecosystems are also stable with respect to cheaters; that is, they resist invasion by species that gain a small growth advantage by ceasing production or degradation of antibiotics. We consider two types of cheating species: those that stop producing antibiotics and revert to intrinsic resistance ($P \rightarrow R_I$) while enjoying production of antibiotic by their parental species, and those that stop degrading antibiotics to become antibiotic sensitive ($R_D \rightarrow S$), yet still enjoying protection by their parental species (Fig. 3a). Starting with a stable 3-species community, we simulated potential cheater invasion by adding a small amount of a cheater species derived from one of the existing species. We calculated the final abundance of a cheater once the community reached steady state while varying the growth advantage of the cheater compared to its parent: $g_i^{cheater} = (1+\varepsilon)g_i$. We assume that each species has a different inherent growth rate, $g_1 < g_2 < g_3$. For small ε, the only cheater that can invade the community is the production cheater derived from the fastest growing strain (Fig. 3b). This cheater replaces its parent, forming a new community of three species interacting through only two antibiotics. Coexistence in this simpler community is robust to parameter variation (Extended Data Fig. 6) and is also evolutionarily stable: it does not allow invasion by cheaters arising from any of its species (Extended Data Fig. 7). All other cheaters in the 3-species 3-antibiotic community cannot invade, even with a small growth advantage (i.e. for small positive ε their final abundance is zero, Fig. 3c). With higher growth advantages, these cheaters can ultimately invade by dominating the community, by replacing the parent in a newly formed 3-species community, or by generating a new 4-species community (Fig. 3c). The emergence of these 4-species communities motivated us to search for more complex ecosystems with greater numbers of species and to explore their dynamical behaviors.

Analysis of more complex networks identified many ways for antibiotic production and degradation to generate stability. Randomly sampling larger networks with up to six species and five antibiotics, we found many stable community topologies, all of which included antibiotic degrading species (Extended Data Fig. 8). Notably, greater numbers of antibiotics generally increase the number of species that can coexist. While the fraction of network topologies that support stable communities can be small, the combinatorial increase in the number of possible networks provides multitudes of ways for antibiotic production and degradation to generate stable communities with large numbers of species. Coexistence among species in these various network topologies can occur through different dynamical behaviors, including stable fixed points, limit cycles, or chaos, depending on the strengths of antibiotic production K_P and degradation K_D (Fig. 4, Extended Data Fig. 9). Thus, in addition to enabling the long-term coexistence of complex communities, the combined effect of antibiotic production and degradation can dramatically impact community dynamics.

Our findings suggest new possibilities for engineering multi-species microbial consortia[30] and shed light on the role of antibiotic production and degradation in maintaining biodiversity within natural microbial communities. Of course, natural microbial ecosystems are extremely complicated[13]: they contain orders of magnitude more species than we modeled and include additional interactions at the level of resource competition, metabolic cross-feeding, phage invasion, and predator-prey relationships. We expect that further

insights into ecosystem stability and assembly will emerge by understanding how these mechanisms generate both pairwise and higher-order multi-species interactions.

Methods

Mixed inhibition-zone model of cyclic 3-species communities

Model description—We derived a formula for the changes of species abundances in the inhibition-zone model for the limit of complete mixing after each time step ($r_{dispersal} \to \infty$) and infinite population size. Let X_i be the abundance of species i per unit area, K_P the killing area around each producer and K_D the degradation area around each degrader. Since species disperse randomly, the fitness f_i of species i depends on its inherent growth rate g_i and the fraction of area 1-p_{kill} in which it is not killed by antibiotics:

$$f_i = g_i \left(1 - p_{kill}\right).$$

For each antibiotic, a sensitive individual S will only be killed if it is located where there is at least one producer P within a K_P neighborhood and there is no protecting R_D species within a K_D neighborhood. Since individuals are randomly placed, the number of cells within such neighborhoods follows a Poisson distribution, so that if λ is the expected number of cells in a region then the probability of having zero cells in the region is $e^{-\lambda}$. Thus the probability of being in the killing zone of P is $1 - e^{-K_P X_P}$, and the probability of not being in the degradation zone of R_D is $e^{-K_D X_D}$ where X_P and X_D are respectively the abundances of species producing and degrading the antibiotic. Combining these we obtain

$$p_{kill} = e^{-K_D X_D}\left(1 - e^{-K_P X_P}\right).$$

Thus for the cyclic 3-species network the fitness of each species is:

$$\begin{aligned} f_1 &= g_1\left(1 - e^{-K_D X_2}\left(1 - e^{-K_P X_3}\right)\right) \\ f_2 &= g_2\left(1 - e^{-K_D X_3}\left(1 - e^{-K_P X_1}\right)\right) \\ f_3 &= g_3\left(1 - e^{-K_D X_1}\left(1 - e^{-K_P X_2}\right)\right). \end{aligned}$$

We update species abundance for each time step using the discrete time formula:

$$X_i\left(t+1\right) = \frac{X_i\left(t\right) f_i\left(t\right)}{\sum_j X_j\left(t\right) f_j\left(t\right)},$$

where the denominator ensures that total species abundance remains constant.

Linear stability analysis—We found the fixed point numerically for each set of parameters and then found the eigenvalues of the Jacobian computed at the fixed point. The logarithm of the maximum absolute value of the eigenvalues was used as a stability measure

in Figure 2b-c to determine the region of stability. The fixed point is stable if this value is less than zero.

Chemostat model of cyclic 3-species communities

Model description—Our chemostat model is adapted from classical models of antibiotic interactions with a constant inflow of a single resource and constant dilution[28]. Ordinary differential equations track the concentration of the resource (Z), the abundances of *3* species (X_i), and the concentrations of *3* antibiotics (C_i), implementing the cyclical interaction network. Each species consumes resources and produce antibiotics. The species degrade antibiotics to which they are resistant, and their growth is inhibited by antibiotics to which they are sensitive. The resource dynamic is:

$$\frac{dZ}{dt} = (Z_o - Z)\, D - \sum_i \frac{X_i G_i}{m},$$

where Z_o is the concentration of the added resource, D is the dilution rate, G_i is the growth rate of species i, and m is a conversion factor between resources and species, so that G_i/m is the resource consumption rate of each species. The species abundances change according to:

$$\frac{dX_i}{dt} = X_i\,(G_i - D) \quad \text{with} \quad G_i = g_i \frac{Z}{k_z + Z} e^{-K_P C_j}.$$

Growth rate increases with the concentration of resources following Monod kinetics, where k_z determines the concentration of half-maximal resource absorption. The growth rate is also affected by antibiotics, decreasing exponentially with the level of antibiotics to which a species is sensitive (here antibiotic C_j inhibits species i). The parameter K_P characterizes the strength of antibiotic inhibition, and g_i is a species-specific maximal growth rate.

The antibiotic concentration dynamics are given by:

$$\frac{dC_j}{dt} = pX_j G_j - K_D X_k C_j - DC_j.$$

The parameter p determines the amount of antibiotics produced per cell division, the second term assumes that species k degrades the antibiotic produced by species j through mass action kinetics, and the parameter K_D characterizes the strength of antibiotic degradation.

Rescaled chemostat model—To analyze the stability of the 3-species 3-antibiotic interaction network, we find the equilibrium levels of resources: summing dX_i/dt and solving for $\sum_i X_i G_i$, substituting into dZ/dt, and finding the steady state to obtain:

$$Z = Z_o - \sum_i \frac{X_i}{m}.$$

We rescale variables to reduce the number of free parameters: time so that $D=1$, Z and k_z so that $Z_o=1$, and we eliminate m by substituting $X_i'=X_i/m$, $C_i'=C_i/m$, $K_P'=mK_P$ and $K_D'=mK_D$. Dropping the primes we obtain:

$$\begin{aligned}\frac{dX_i}{dt} &= X_i\left(G_i-1\right)\\ G_i &= g_i\frac{1-\sum_i X_i}{k_s+1-\sum_i X_i}e^{-K_P C_j}\\ \frac{dC_j}{dt} &= pX_jG_j-K_DX_kC_j-C_j.\end{aligned}$$

Linear stability analysis—The problem of finding the fixed point in the rescaled model was reduced to a single non-linear algebraic equation, which was numerically solved for different parameters to determine the corresponding equilibriums for X_i and C_i. At the fixed point $\frac{dX_i}{dt}=0$ and therefore $G_i = 1$. This allows us to express the C_j's as functions of

$$\Theta=\frac{1-\sum_i X_i}{k_s+1-\sum_i X_i}$$

and the g_i's. Substituting the expressions for C_j into

$$pX_jG_j-K_DX_kC_j-C_j=0$$

results in a system of linear equations for X_i's, which can be solved as a function of Θ. This allows us to express $\sum_i X_i$ as a function of Θ and thus obtain a non-linear equation for Θ. For Extended Data Figure 5a, the stability of the fixed point was determined by finding the eigenvalues of the Jacobian at the fixed point. A negative largest real component of the eigenvalues indicates stability.

Robustness to mutation and invasion by cheating species

Each cheating species c was cloned from a parent p by copying all antibiotic phenotypes except for a mutation in the phenotype with respect to a single antibiotic: $P\rightarrow R_I$ for production cheaters, and $R_D\rightarrow S$ for degradation cheaters. Starting with a 3-species community at equilibrium, we added a small amount of the cheating species ($X_c = 0.001$, with abundances of the other species renormalized so that $\sum_i X_i = 1$). We set the growth rate of the cheater to the parental growth rate with a growth advantage ε, so that $g_c = (1+\varepsilon)g_p$. We ran each simulation until species abundances reached steady state or stable oscillations, and then we calculated the minimum and maximum values for each cheater during the last third of the simulation time.

Coexistence of communities with 3 species and 2 antibiotics

Cyclic 3-species communities maintain coexistence even when the fastest growing species ceases antibiotic production, resulting in a simpler 3-species 2-antibiotic community. This network exhibits robust coexistence similar to the 3-antibiotic network, so long as the species that does not produce antibiotics is the fastest growing species (Extended Data

Figure 6a). This simpler community also resists invasion by any remaining production or degradation cheaters (Extended Data Figure 7b).

We investigated whether further reductions of this network support coexistence. While coexistence is possible when only one of the two antibiotics is degraded, this coexistence occurs only for a small range of parameter values (Extended Data Figure 6b). Based on a comprehensive sampling of parameter space, we found that further reductions to communities that produce only a single antibiotic do not support coexistence when inherent growth rates differ. This is consistent with the intuition that when only one antibiotic is being produced there will always be two species that are equivalent with respect to the antibiotic, which will lead to extinction of the slower growing species. Thus, in contrast to spatial models where coexistence is possible on a single antibiotic[11], coexistence in well-mixed models requires 3 species and at least 2 antibiotics.

Generalizing the mixed inhibition-zone model for arbitrary interaction networks

Model description—We calculated the probability of each species being inhibited for a general ecosystem with N_s species and N_a antibiotics, where species can be any of the 4 antibiotic phenotypes (P, S, R_I or R_D) for each antibiotic. The assumptions are the same as for the mixed inhibition-zone model of cyclic 3-species communities. Consider the situation in which antibiotic production is stronger than degradation ($K_P > K_D$, the other scenario follows similarly). For an individual of a target sensitive species, each of the other $N_s - 1$ species can be either near enough to affect the target through production and degradation of some of the antibiotics (with probability p_{near}), can be at intermediate distances in which they affect the target through production but not degradation ($p_{intermediate}$), or can be far away so that they do not affect the target in any way (p_{far}). These 3 distance ranges make for 3^{N_S-1} possible combinations for the presence or absence of the other species within any neighborhood of the target species. Based on the phenotypes of the sensitive target species and the other species, we calculated all combinations that result in antibiotic inhibition. For each species i, we calculated the probabilities p_{near}, $p_{intermediate}$ and p_{far} from the levels of production and degradation of the antibiotics, in this case:

$$\begin{aligned} p_{near} &= 1 - e^{-K_D X_i} \\ p_{far} &= e^{-K_P X_i} \\ p_{intermediate} &= p_{far} - p_{near}. \end{aligned}$$

Combining these, we calculated the probability p_c of each inhibitory combination occurring, multiplying the probabilities of each species being either near, intermediate, or far according to the requirements of each combination. Finally, we obtained the total probability of the target species being inhibited by summing across all possible inhibitory combinations with $p_{kill} = \sum_c p_c$. As in the 3-species model we let the fitness of each species be:

$$f_i = g_i (1 - p_{kill})$$

and

$$X_i(t+1) = \frac{X_i(t) f_i(t)}{\sum_j X_j(t) f_j(t)}.$$

Testing for coexistence in more complex networks

We randomly sampled up to 10^6 networks for each combination of 4-6 initial species and 1-5 initial antibiotics by randomly choosing one of the four phenotypes (S, P, R_I or R_D) for each species/antibiotic combination. When the total number of possible networks was less than 10^6 we tested all networks. We excluded networks that contained antibiotics or species with identical properties from subsequent simulations, since these are equivalent to instances of networks with a smaller number of antibiotics or species. With N_a initial antibiotics and N_s initial species at initial abundances $1/N_s$, we calculated the number of final species surviving at abundance $X_i > 0.01/N_s$ after 10,000 time steps. Simulations were binned by the maximum number of surviving species across all possible combinations of the parameters: $g_{max} = \{1.2$ or $2.5\}$, $K_P = \{10$ or $30\}$ and $K_D = \{3$ or $10\}$. For a given g_{max}, species growth rates were evenly spaced between 1.0 and g_{max}. With total number of network topologies $N_{total} = 4^{N_s N_a}/N_a!$, even this sparse sampling of parameters shows that the total number of topologies that support stability is quite large (Extended Data Figure 8).

Calculating effective number of species using Shannon diversity

We calculated effective species numbers by the Shannon entropy H of the species distribution:

$$H = -\sum_i X_i \log_2 X_i$$

with species frequencies X_i normalized such that $\sum_i X_i = 1$. Effective number of species is then given by 2^H.

Parameter values for main text figures

Figure 1: Grids were 200×200 with wrapping boundaries. Species were initially randomly seeded on the grid at low total abundance (*1%*), or in an initial configuration with 3 large domains for $r_{dispersal} > 20$ to reduce the initial chance of extinction of all species at high levels of mixing (with intrinsic resistance). (**e**) Lines show average of 10 simulations, calculating the effective species numbers based on Shannon diversity of species within 40×40 subregions (shown in insets) at 100 evenly spaced locations on the grid at the final time; other parameters: $r_{production} = 3$, $r_{degradation} = 3$, $r_{dispersal} = \{3, 4, 6, 10, 20, 80, 200\}$; runtimes for each $r_{dispersal}$ are respectively: $\{150, 150, 75, 75, 75, 25, 25\}$, after which the overall spatial patterns were relatively unchanging. For intrinsic resistance with $r_{dispersal} = \{80, 200\}$ it was possible for all species to be inhibited at the same time step, in which case we choose one cell at random to proceed to the next generation.

Figure 2: We estimated the size of the basin of attraction by running simulations starting from 210 different initial species abundances that were equally spaced on a triangle lattice inside the $x_1+x_2+x_3=1$ two-dimensional simplex. The basin of attraction area is the fraction

of simulations that move to the fixed point with all three species coexisting. **a**, $g_1 = 1.0$, $g_2 = 1.1$, $g_3 = 1.2$; left: $K_P = 4$, $K_D = 0$; right: $K_P = 12$, $K_D = 3$. **b**, left: $K_P = 4$, $K_D = 0$; right: $K_P = 40$, $K_D = 4$. **c**, $g_1 = 1$, $g_2 = 3$, $g_3 = 2$.

Figure 3: $g_1 = 1.0$, $g_2 = 1.1$, $g_3 = 1.2$, $K_P = 16$, $K_D = 4$.

Figure 4: $g_1 = 1.0$, $g_2 = 1+1/30$, $g_3 = 1+2/30$, $g_4 = 1.1$; stable equilibrium: $K_P = 10$, $K_D = 10$; limit cycles: $K_P = 12$, $K_D = 20$; chaos: $K_P = 20$, $K_D = 55$.

Code availability

MATLAB code for the spatial inhibition-zone model, mixed inhibition-zone model and chemostat model is available from the authors upon request.

Note on the mechanism of 3-way attenuating interactions

Antibiotic degradation is a common mechanism of antibiotic resistance[21] and is therefore a probable mechanism for the attenuation of inhibition that we observed in the 3-species interaction assays and the antibiotic modulation assays (Extended Data Figures 1-2). There is strong evidence in support of this assumption based on many reports of antibiotic degrading species protecting sensitive species from antibiotics[20,25,26,31-33]. Antibiotic degradation is also a known mechanism of resistance for the antibiotics in which we observed significant attenuation (Extended Data Figure 1c): tobramycin[34], ciprofloxacin[35], β-lactam antibiotics[36] (foxicilin, pipericillin, penicillin), nitrofurantoin[37], rifampin[38] and trimethoprim[32]. Furthermore, we experimentally confirmed that degradation through β-lactamases contributes to the attenuation of β-lactam antibiotics through a modified version of the antibiotic modulation assays that uses β-lactamase inhibitors (Extended Data Figure 1d, Extended Data Figure 2c). However, we note that the models we use can be easily generalized to additional mechanisms that generate antibiotic-attenuation, for example through antibiotic suppression[24,39].

Interaction experiments

3-species interaction assays—All possible pairings of 16 *Streptomyces* species from a spore collection (~100 spores/μL) were pinned 1 cm apart on 9 cm petri dishes with 1x oatmeal agar, and plates were grown in a darkened plastic bin for 13 days at room temperature. Overlay media without thiamine was prepared in test tubes in 5mL aliquots, melted in an autoclave (to melt, not sterilize), and cooled to 42° C in a water bath. An overnight LB culture of *E. coli* expressing YFP was mixed 9:1 with 1000x thiamine stock, 50μL of the *E. coli* mixture was added to overlay agar, quickly vortexed to mix and then poured uniformly onto the plate. Plates were incubated at 37° C for 18 hours and photographed in bright field and YFP channels to record the antibiotic inhibition-zone. Combinations in which one species created a large inhibition-zone were scored using the modulation index $M = (r_m - r_o)/(r_m + r_o)$, where r_m is the radius of the inhibition-zone in the direction of the modulator and r_o is the radius of the inhibition-zone in the opposite direction. Extended Data Figure 1b shows data from 54 combinations in which one species made a large inhibition-zone, with 5 antibiotic producers and 11 modulator species (1 plate removed due to contamination). Extended Data Figure 2a shows images and scoring. We

observed similar attenuation in follow-up technical replicas of individual strain combinations and when testing on other media.

Antibiotic modulation assays—Antibiotic modulation assays were similar to the 3-species assays except that the antibiotic producing species was replaced with pure antibiotic and the assay geometry was modified to enable more high-throughput measurements. Modulator inoculation plates were prepared by spreading 50 μL of 20% glycerol spore stocks onto 1/2x oatmeal agar 9 cm petri dishes with glass beads, incubated 1 week at 30° C in plastic bins, then stored at room temperature. 25 mL of 1/2x Oatmeal agar was spread evenly over a 14 cm petri dish. On day 1, a small amount of antibiotic stock was pipetted onto the center of the agar, absorbed and stored at 30° C (cefoxitin 10 μL, chloramphenicol 10 μL, ciprofloxacin 10 μL, doxycyclin 10 μL, nitrofurantoin 20 μL, penicillin 20 μL, piperacillin 15 μL, rifampicin 20 μL, tobramycin 40 μL, trimethoprim 20 μL). On day 2, a thin radial line for each of three modulator species was inoculated using the edges of sterilized 60 mm cover glass (VWR 48393-070) onto the 14 cm petri dish. Plates were incubated in plastic bins at 30° C for three days and small areas of contamination were cutout of the agar. Overlay media was prepared in 25mL aliquots, as in the 3-species assays. Overnight cultures of yellow fluorescent protein (YFP) and cyan fluorescent protein (CFP) producing *E. coli* were combined at equal ratios (by OD) and mixed 9:1 with 1000x thiamine stock. 1mL of the *E. coli* mixture was added to the overlay media, vortexed, and poured evenly over the surface of the oatmeal agar. All plates were incubated at 37° C between 16-21 hours and photographed in bright field, YFP and CFP channels to record the antibiotic inhibition-zone. Test strains included the two strongest attenuators from the 3-species assay, *Streptomyces coelicolor* and a collection of soil isolates from Massachusetts and Colorado soils. Combinations were marked with a dot for significance in Extended Data Figure 1c where the average modulation index M deviated from 0 by at least twice the standard error in the mean ($p<0.05$, two-sided t-test, $N=3$ technical replicas). These images were also visually inspected to confirm warping of the inhibition-zone boundary. Extended Data Figure 2b shows examples and scoring for different antibiotics.

β-lactamase inhibitor assays—1mL of 1mM β-lactamase inhibitor was spread evenly over 14cm 1/2x Oatmeal plates with glass beads and allowed to dry in a ventilation hood (to minimize contamination). Overlay with YFP and CFP *E. coli* was the same as the antibiotic modulation assay except that 1mL of 1mM β-lactamase inhibitor stock was added to the overlay media and vortexed prior to adding *E. coli*. Extended Data Figure 1d shows data for a collection of 14 species, 4 antibiotics and 3 beta-lactamase inhibitors. Extended Data Figure 2c shows example assay images.

Isolation of soil bacteria—Isolation and identification of 5 *Streptomyces* from soil A (Massachusetts) as described in Vetsigian et al[17]. We chose 5 strains from a collection of 47 isolates that did not produce strong antibiotic inhibition-zones on oatmeal agar. Soil B (Colorado) was collected from White River National Forest in unincorporated Pitkin County. We chose 10 strains from a collection of 55 isolates that did not produce strong inhibition-zones, including 2 *Streptomyces* species, 5 Actinobacteria species and 3 non-

Actinobacteria species. Species identification was through Sanger sequencing of 16S ribosomal DNA.

Imaging and data analysis—The 3-species assay images were photographed using a custom-built automated fluorescent imaging system as described in Chait et al[40]. Other assays were using a similar but newer system. Levels of antibiotic modulation were scored by manually recording the edges of the inhibition-zones of the fluorescent *E. coli* using MATLAB. Example images were normalized to fill the dynamic range and gamma adjusted to improve contrast.

Growth media—1x oatmeal agar: 72.5 g/L Difco oatmeal agar (BD). 1/2x oatmeal agar: 31.25 g/L Difco Oatmeal Agar (BD) and 6.25 g/L Bacto agar (BD), with ~100 μL/L 10M NaOH to adjust to pH 7. Media for overlays consisted of M63 salts (2 g/L $(NH_4)_2SO_4$, 13.6 g/L KH_2PO_4, 0.5 mg/L $FeSO_47H_2O$) supplemented with 0.4% glucose, 0.02% casamino acids, 1 mM $MgSO_4$, 1.5 mM thiamine, 7.5g/L bacto-agar (BD), adjusting pH to 7.0 with 1M NaOH. 1000x Thiamine was prepared at 1.5 M in H_2O and filter sterilized.

Chemical stocks—cefoxitin (Sigma C-4786) 50 mg/mL in H_2O, chloramphenicol (Sigma C0378) 30 mg/mL in EtOH, ciprofloxacin (Sigma 17850) 10 mg/mL in H_2O+3uL/mL 10M HCl, doxycyclin (Sigma D-9891) 50 mg/mL in H_2O, nitrofurantoin (Sigma N7878) 10 mg/mL in DMF, penicillin (Sigma 13750) 50 mg/mL in H_2O, piperacillin (Sigma P8396) 50 mg/mL in H_2O, rifampicin (Sigma R3501) 16 mg/mL in DMSO, tobramycin (Sigma T4014) 50 mg/mL in H_2O, and trimethoprim (Sigma T7883) 5 mg/mL in H_2O. β-lactamase inhibitors were prepared at 1mM in H_2O: clavulanic acid (as potassium clavulanate, Sigma 33454), tazobactam sodium salt (Sigma T2820), sulbactam (Sigma S9701).

Extended Data

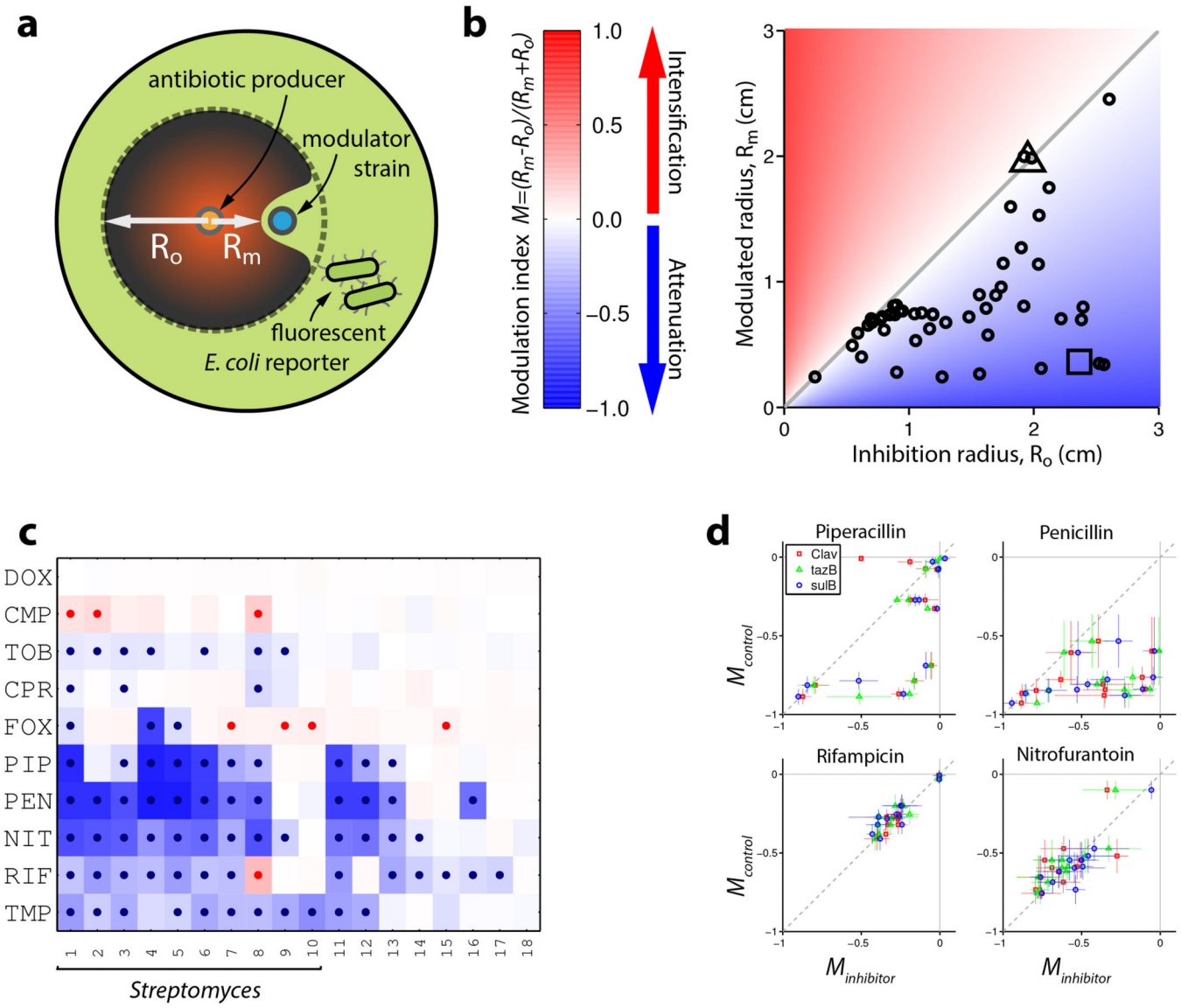

Extended Data Figure 1. Antibiotic attenuation is widespread among natural antibiotic producing species isolated from soil

a, Diagram of 3-species assays: measuring the antibiotic inhibition-zone of *E. coli* around a producer strain enables quantification of 3-species interactions caused by a modulator strain. **b**, Attenuating interactions dominate among a set of 54 *Streptomyces* producer-modulator combinations. Triangle and square markers show scoring from example images in Figure 1b, left and right respectively. **c**, Antibiotic modulation assays: attenuating interactions dominate among combinations of soil species with a panel of 10 pure antibiotics. Combinations are colored by modulation index as in panel b and marked with a dot where the modulation index is significantly different from zero ($N=3$, Methods). Strains 1 and 2 are the strongest modulators from the 3-species assays, strain 3 is *Streptomyces coelicolor*, strains 4-18 are additional soil isolates (Extended Data Table 1). Antibiotics:

doxycycline=DOX, chloramphenicol=CMP, tobramycin=TOB, ciprofloxacin=CPR, cefoxitin=FOX, piperacillin=PIP, penicillin=PEN, nitrofurantoin=NIT, rifampicin=RIF, trimethoprim=TMP. d, Scatter plots of average modulation index *M* for 12 species from panel **c**, with and without β-lactamase inhibitors. Points occur off the diagonal for the β-lactams piperacillin and penicillin but near the diagonal for the structurally unrelated antibiotics rifampin and nitrofurantoin, consistent with attenuation of the β-lactams through a mechanism of antibiotic degradation. Error bars are standard error of the mean for technical replicas with inhibitor (*N=3*) or without inhibitor (control, *N=6*). Control is addition of H_2O instead of inhibitor. Clav=clavulanic acid, tazB=tazobactum, sulB=sulbactam.

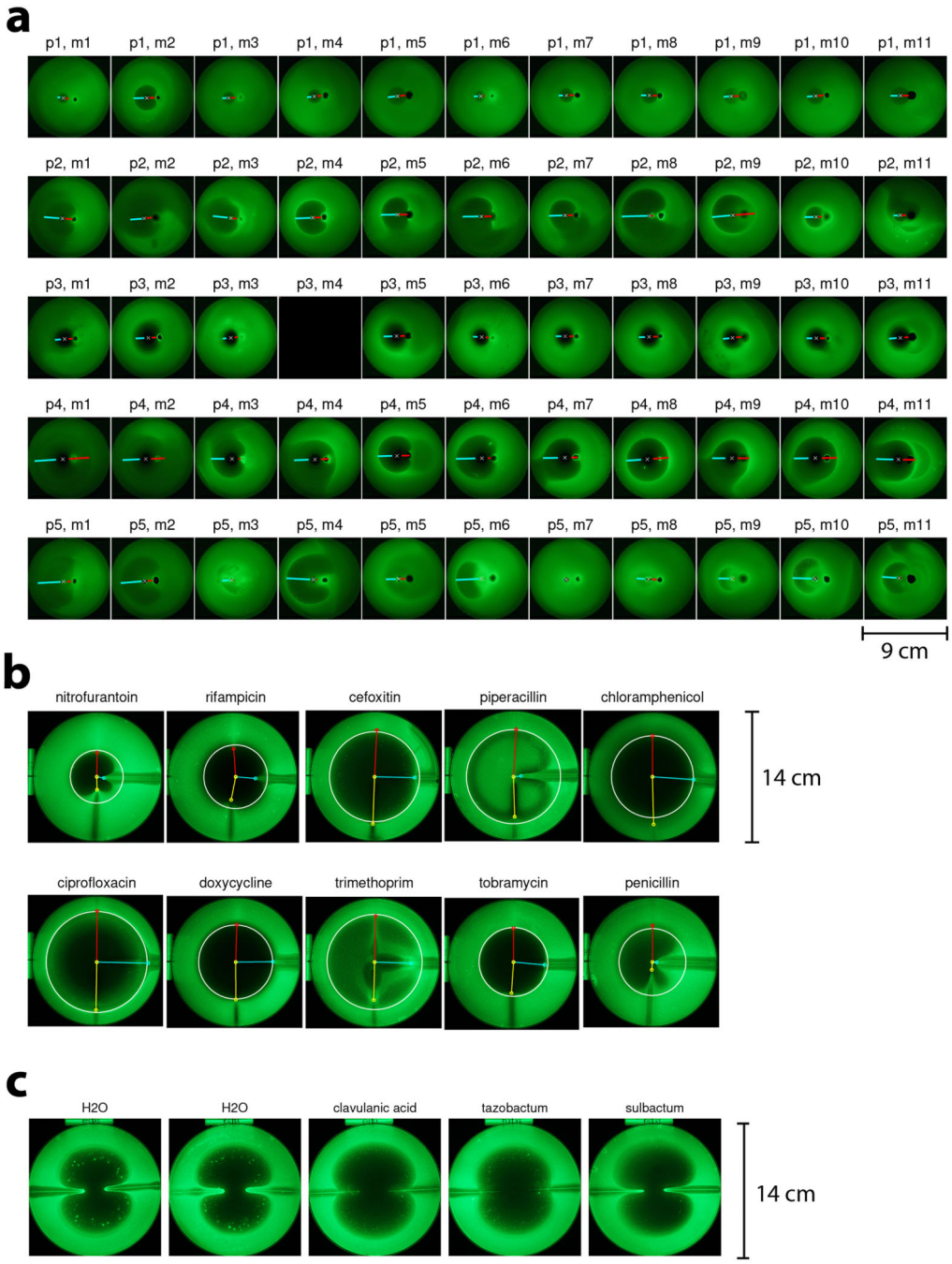

Extended Data Figure 2. Example images from 3-species interaction assays and antibiotic assays

a, Images and scoring for 3-species interaction assays from Extended Data Figure 1b. **b**, Example images and scoring from the antibiotic modulation assays from Extended Data Figure 1c. Each plate shows tests for modulation of antibiotic inhibition for 3 different species against a different antibiotic. Color lines show the size of the inhibition-zone at the location of the radially positioned modulator species; the white circle show the radius of the zone of inhibition as inferred from the left side of the plate that contains no modulators. **c**, Example images from an antibiotic modulation assay with β-lactamase inhibitors and the β-

lactam antibiotic cefoxitin. Left and right side of each plate is inoculated with a line of species 4 from Extended Data Figure 1c. Attenuation is significantly reduced by the β-lactamase inhibitors (especially clavulanic acid and tazobactam) when compared to controls (H_2O).

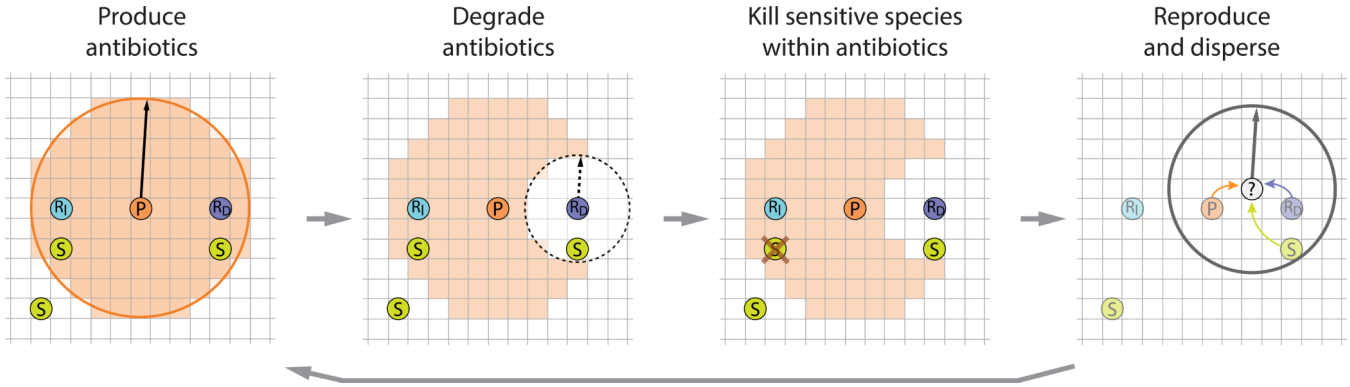

Extended Data Figure 3. Illustration of the spatial inhibition-zone model

The simulation is performed on a grid of size *LxL*. A single individual occupies each grid location. During each generation: 1) Individuals from species of type *P* produce antibiotics within a circle of radius $r_{production}$. 2) Individuals of type R_D remove antibiotics within a circle of radius $r_{degradation}$. This process is repeated for each of the different antibiotics. 3) All sensitive individuals (type *S*) are killed at any locations that still contain the corresponding antibiotics (crossed out S; antibiotic values at each location are calculated at center positions). 4) Empty locations of a new grid are filled by randomly choosing from any surviving individuals within a radius $r_{dispersal}$. If there are no surviving individuals within $r_{dispersal}$ then an empty location remains empty.

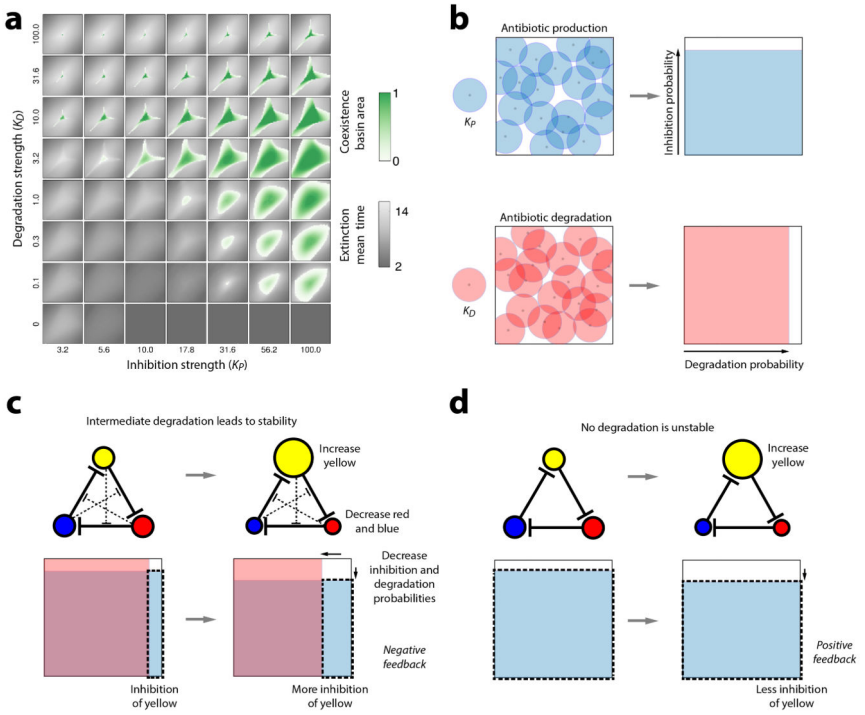

Extended Data Figure 4. Dependence of coexistence on degradation in the mixed inhibition-zone model

a, Stability analysis of the full parameter space in the mixed inhibition-zone model. Using simulations, we tested the stability of cyclic 3-species 3-antibiotic communities with dense sampling of all possible parameters for the inhibition-zone model, varying strengths of K_P and K_D, initial abundances of species 1-3 and growth ratios g_2/g_1 and g_3/g_1. As in Figure 2b, each grid shows a 100 fold range of growth rate ratios from 0.1 to 10. Large basins of attraction exist across a wide range of parameter values, with maximal stability at high levels of antibiotic production and intermediate levels of degradation. **b-d**, Intuition for why coexistence depends on degradation. **b**, the inhibition-zone model calculates the probability of a given sensitive species being inhibited by an antibiotic producer (blue), or being protected by a degrading species (red), given the relative strengths of production (K_P) and degradation (K_D). The expected area covered by the overlapping circles (left) is used to calculate the corresponding inhibition and attenuation probabilities (percentage area of filled boxes, right; Methods). **c**, Focusing on one antibiotic in a stable 3-species community: increasing the abundance of the yellow species creates negative feedback by decreasing the abundance of blue and red, which results in more inhibition of yellow. **d**, Communities are not stable at low levels of degradation due to positive feedback, whereby increasing the abundance of the yellow species results in a decrease of inhibition.

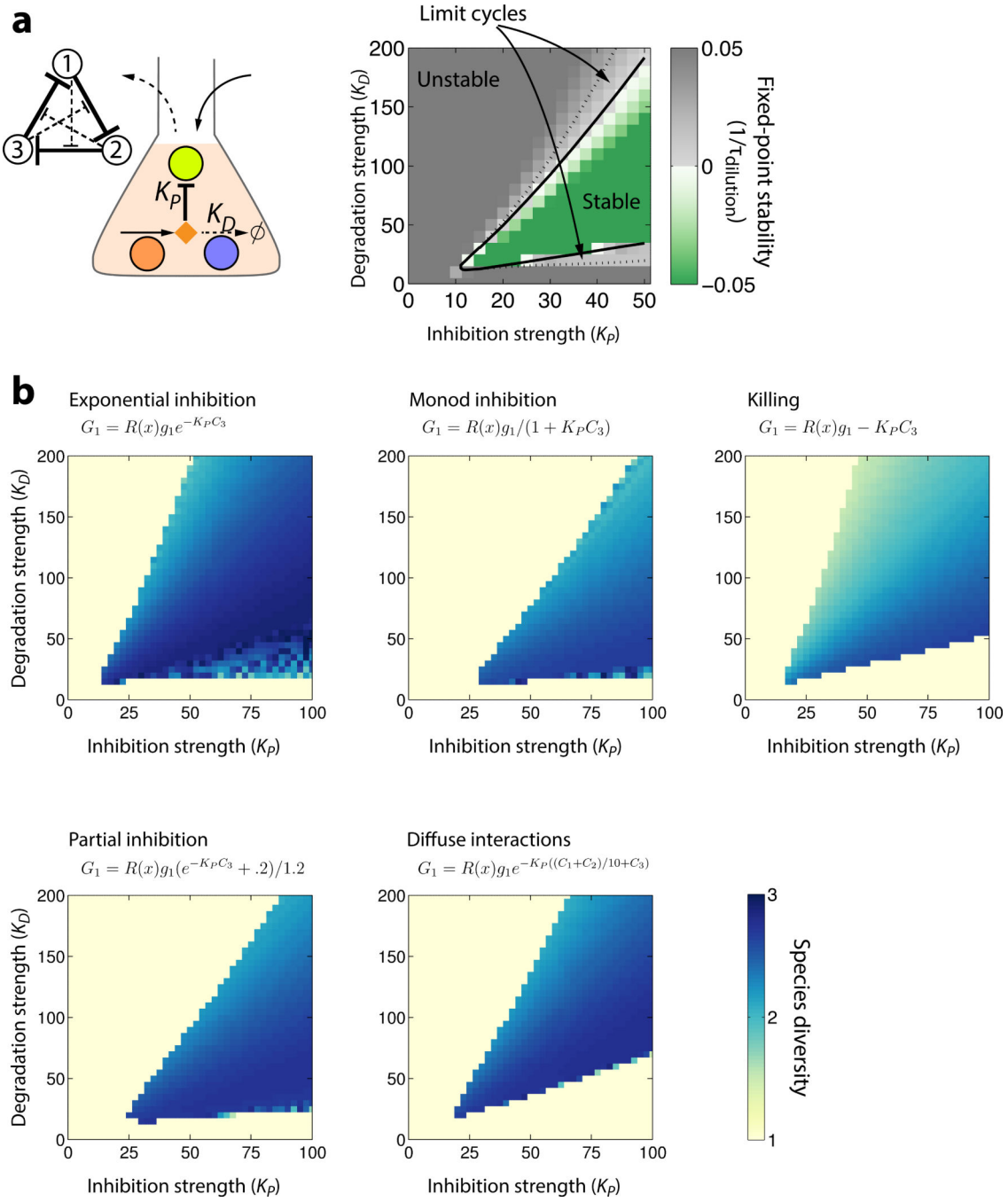

Extended Data Figure 5. Coexistence of antibiotic degrading communities in a well-mixed chemostat model with three antibiotics

a, Stability of the 3-species 3-antibiotic community in a single resource chemostat model in which species and antibiotics are completely homogeneous. Communities in the chemostat model may coexist through fixed points or limit cycles. For parameter sets in which the fixed point of the chemostat model was unstable, we started simulations close to the fixed point to determine if the community coexists through a limit cycle. Limit cycles occur in the areas between the dashed and solid black lines. Chemostat parameters: $g_1 = 3$, $g_2 = 6$, $g_2 =$

9, $k_s = 0.5$, $p = 1$. **b**, Communities coexist in the chemostat for a wide range of assumptions regarding antibiotic mechanisms. We simulated the chemostat model while changing how the action of the antibiotics is modeled and observed robust coexistence across all models. For each simulation we started all species at equal concentration ($X_i = 0.2$), ran the simulation until $t = 100$ and calculated the Shannon diversity of the final species levels. The default chemostat model assumes exponential inhibition of species by antibiotics, but similar coexistence is observed for Monod-like inhibition, species killing instead of inhibition, when species are only partially inhibited or when each species is sensitive at some level to all antibiotics. G_1 is the growth rate of species 1 under inhibition, while g_1 is its maximal rate of growth; $R(x)$ captures resource dependence on current species levels; C_1, C_2 and C_3 are the concentrations of antibiotics produced by species 1-3 respectively (Methods). Equations for the growth of species 2 and 3 have the same form as G_1. All other parameters are the same as for panel **a**.

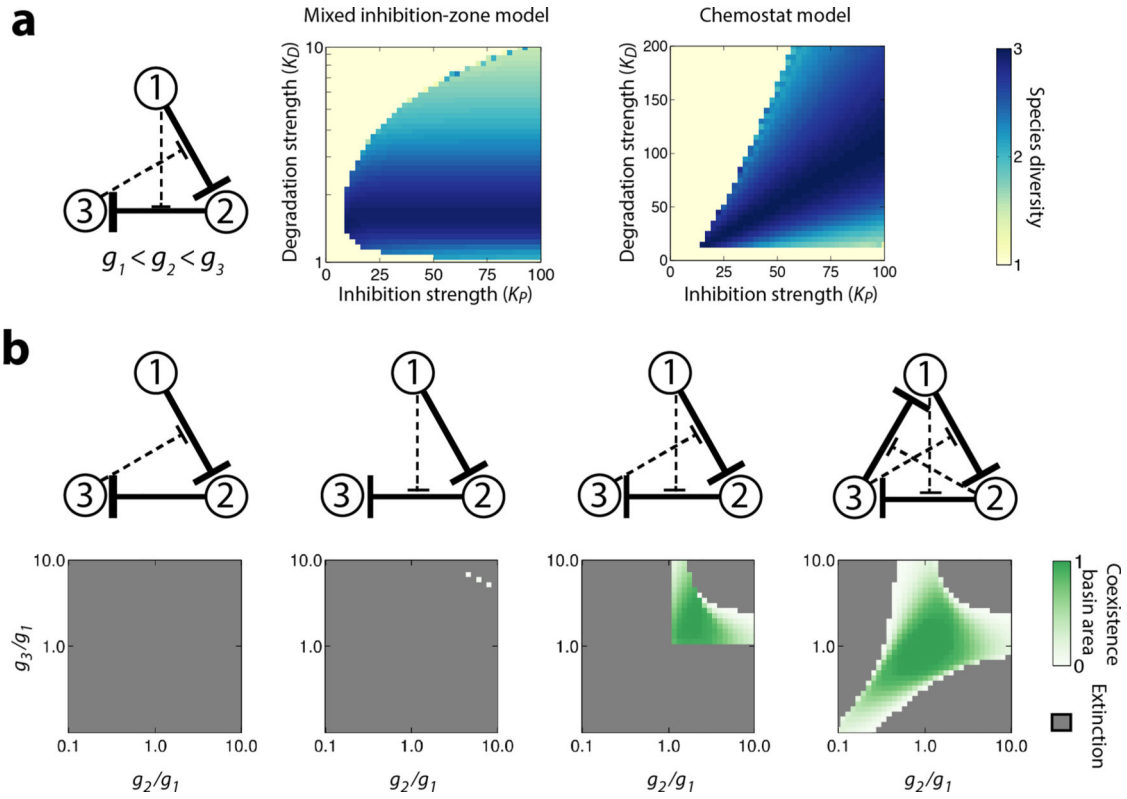

Extended Data Figure 6. Coexistence of communities with three species and two antibiotics

a, Comparing community diversity in the mixed inhibition-zone model and the chemostat model. For each simulation we started all species at equal concentration ($X_i = 1/3$ for the inhibition-zone model, $X_i = 0.2$ for the chemostat model), ran the simulation for time 100 and calculated the Shannon diversity of the final species levels. Other parameters are the same as in Figure 2 for the inhibition-zone model or Extended Data Figure 5 for the chemostat model. **b**, Three species communities require two antibiotics for stability. When only one antibiotic is degraded the community either lacks stability (first panel), or is stable only for a small number of growth rates and initial conditions (second panel). When two

antibiotics are degraded the community is robustly stable to differences in species growth rates and initial conditions (third panel), provided that the antibiotics inhibit the faster growing species (species 2 and 3). Basin colors as in Figure 2b; gray shows parameters for which no initial conditions were stable; $K_P = 40$, $K_D = 4$.

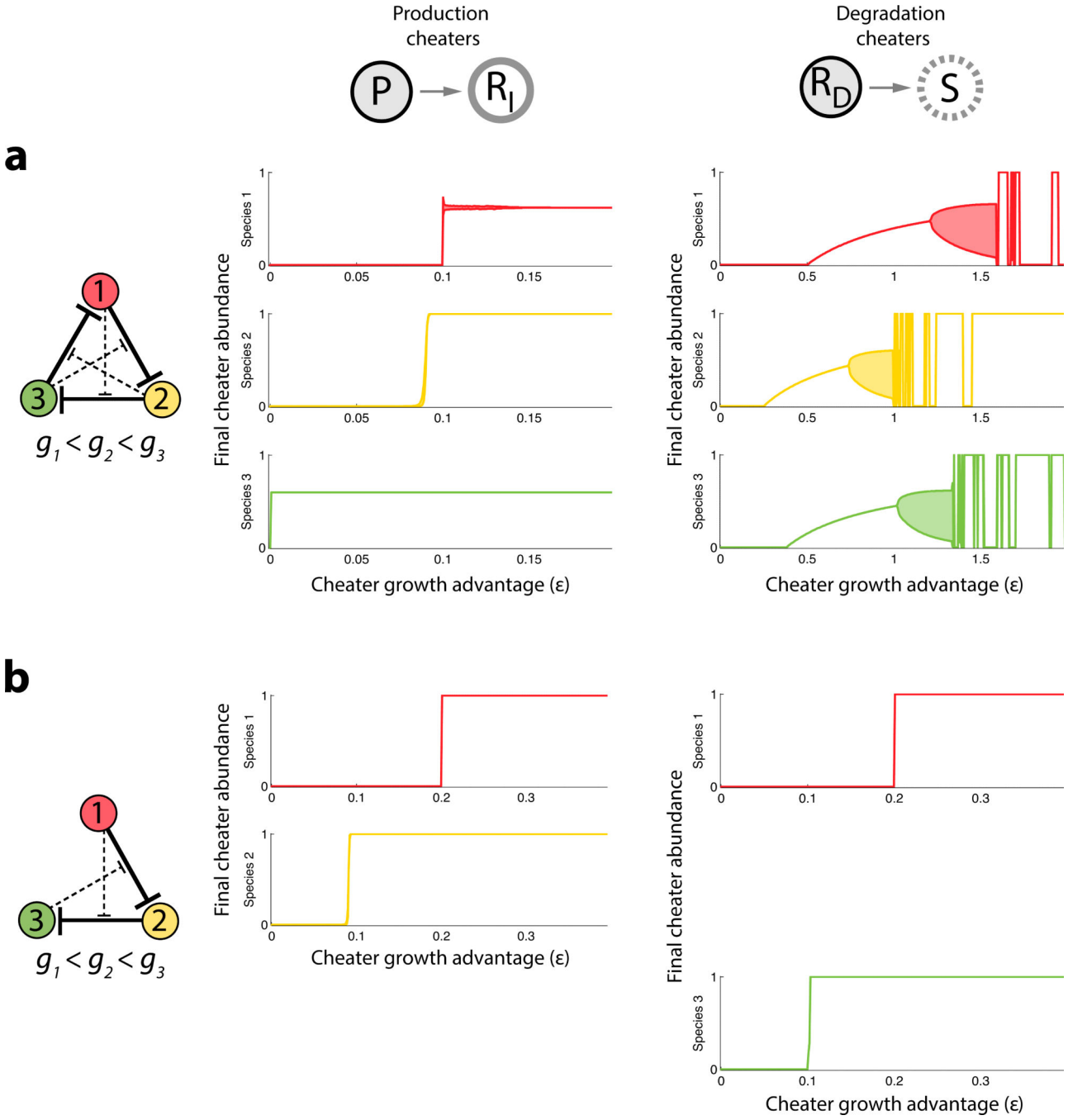

Extended Data Figure 7. Robustness of three species communities to invasion by cheaters in the mixed inhibition-zone model

Analysis of production cheaters ($P \rightarrow R_I$, left) and degradation cheaters ($R_D \rightarrow S$, right). As in Figure 3, we plot the final abundance of each cheater as a function of its growth advantage ε

over its parent species. **a**, Cheaters cannot invade the 3-species 3-antibiotic network when their growth advantage is small, except for the production cheater of the species with the fastest inherent growth rate (species 3, green line), which replaces its parent generating a new stable community of 3 species interacting through 2 antibiotics. **b**, This resulting 3-species 2-antibiotic community is resilient to invasion by all cheaters; cheaters must have a substantial growth advantage to invade and take over. Parameters for both networks are the same as Figure 3. Shaded areas indicate the maximum and minimum abundance when the community reaches stable oscillations.

Note: The analysis above is for networks with $g_1 < g_2 < g_3$. The alternative network of $g_1 > g_2 > g_3$, is less robust to cheater invasion. Two cheaters can invade this community even with small ε: the production cheater for species 2, which gives rise to a stable 3-species 2-antibiotic community, and the production cheater of species 1, which takes over the community.

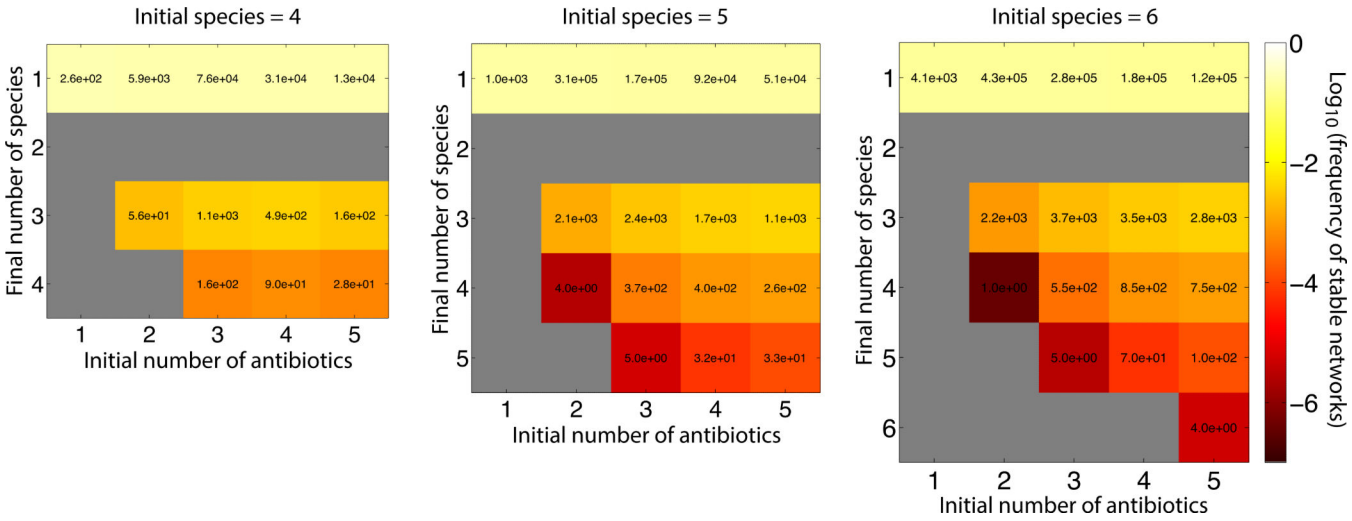

Extended Data Figure 8. Complex network topologies support coexistence of larger numbers of species in the mixed inhibition-zone model

For given initial numbers of species and antibiotics, sets of up to 10^6 communities with random networks were simulated and the final number of surviving species recorded. The number inside each square shows how many networks resulted in the specified number of final species (after removing networks that did not use all of the initial antibiotics, Methods). Colors show the frequency of each outcome within all simulated networks, with gray where no stable networks were found. We sparsely sampled parameters for species growth rates and antibiotic production and degradation levels (Methods). The sparse sampling means that a given network topology may exhibit stability for parameter combinations that were not tested.

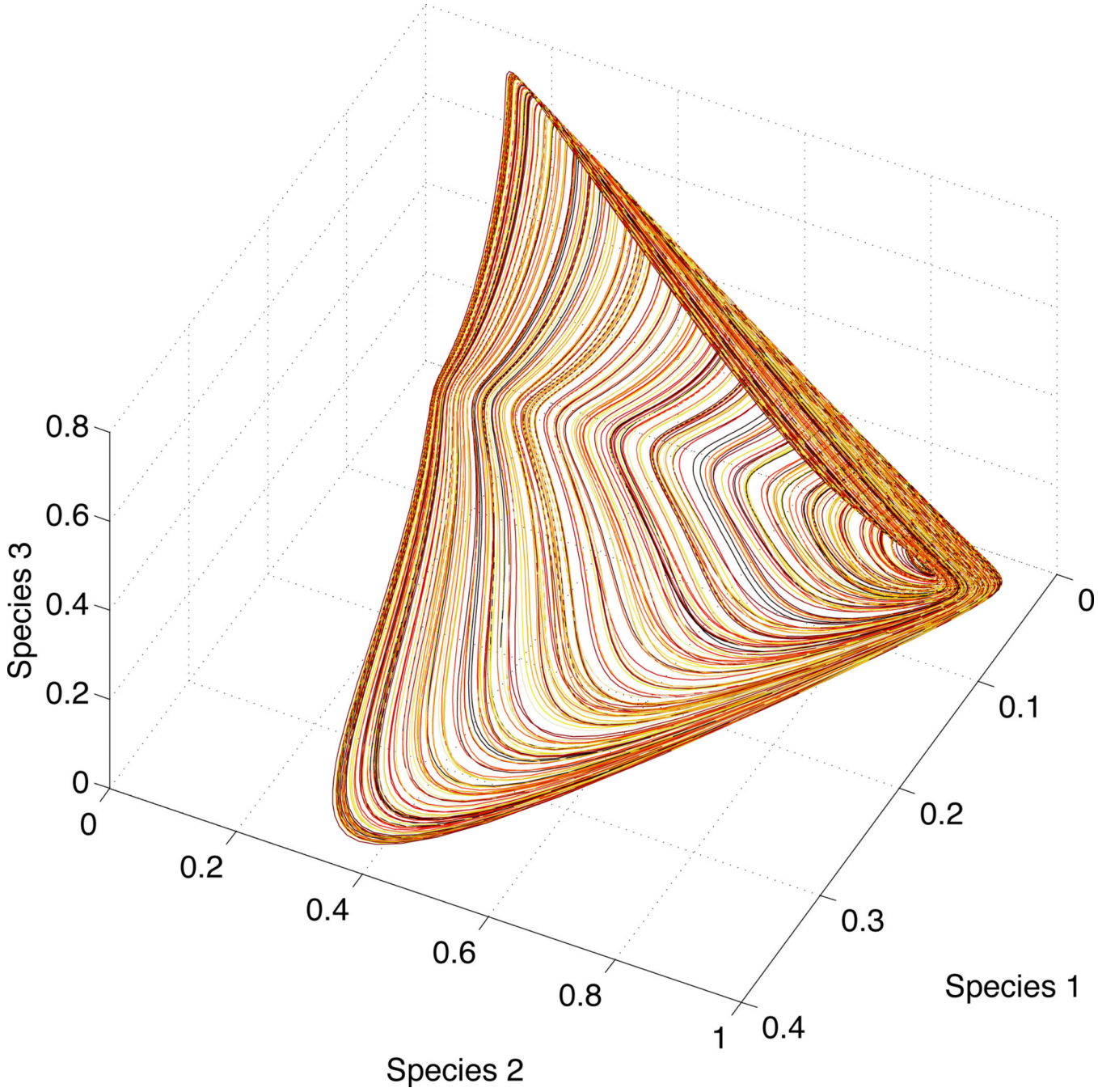

Extended Data Figure 9. A community with chaotic dynamics

Plotting the abundance of species 1-3 for the network from Figure 4b. We show the last 30,000 steps of a length 40,000 time-series, colored with a slowly changing gradient. The trajectories form a strange attractor.

Extended Data Table 1

Strain information for experimental assays.

ED Fig. 1b ED Fig. 2	ED Fig. 1c	Species	Notes	Assays
p1		*Kutzneria sp. 744*	producer	1
p2		*Streptomyces clavuligerus* (ATCC 27064)	producer	1
p3		*Streptomyces sviceus* (ATCC 29083)	producer	1
p4		*Streptomyces sp. Mg1*	producer	1
p5		*Streptomyces albus* (J1074)	producer	1
m1		*Streptomyces SPB74*		1
m2		*Streptomyces griseoflavus* Tu4000		1
m3		*Streptomyces sp. AA#4*		1
m4	1	*Streptomyces pristinispiralis (ATCC 25486)*		1, 2, 3
m5		*Streptomyces hygroscopicus* (ATCC 53653)		1
m6		*Streptomyces SPB78*		1
m7		*Streptomyces ghanaensis* (ATCC 14672)		1
m8	2	*Streptomyces roseosporus (NRRL 11379)*		1, 2, 3
m9		*Streptomyces viridochromogenes* (DSM 40736)		1
m10		*Streptomyces lividans* (TK24)		1
m11		*Streptomyces sp. E14*		1
	3	*Streptomyces coelicolor*		2, 3
	4	*Streptomyces sp. G1-4*, JN020492	soil A	2, 3
	5	*Kitasatospora sp. G4-12*, JN020549	soil A	2, 3
	6	*Streptomyces sp. G2-6*, JN020526	soil A	2, 3
	7	Unclassified *Streptomycetaceae*	soil B	2, 3
	8	*Streptomyces sp. G4-8*, JN020545	soil A	2, 3
	9	*Streptomyces sp. G1-14*	soil A	2
	10	*Streptomyces sp. RI18-DHHV3*	soil B	2
	11	*Amycolatopsis sp.*	soil B, Actinobacteria	2, 3
	12	*Kribbella sp. NBRC 104208*	soil B, Actinobacteria	2, 3
	13	*Rhodococcus sp.*	soil B, Actinobacteria	2, 3
	14	*Microbacterium sp.*	soil B, Actinobacteria	2
	15	*Rhodococcus sp. 602*	soil B, Actinobacteria	2
	16	*Agromonas sp.*	soil B, Alphaproteobacteria	2, 3
	17	*Lysobacter sp.*	soil B, Gammaproteobacteria	2
	18	*Bradyrhizobiaceae Bosea*	soil B, Alphaproteobacteria	2
S		*E. coli* MC4100-YFP/pCS-l	assay strain w/ chromosomal YFP	1
	S	*E. coli* MC4100, pZS2R-YFP	assay strain w/ YFP plasmid	2, 3

ED Fig. 1b ED Fig. 2	ED Fig. 1c	Species	Notes	Assays
	S	*E. coli* MC4100, pZS2R-CFP	assay strain w/ CFP plasmid	2, 3

Assay numbers: 1=Three-species interaction assay, 2=Antibiotic modulation assay, 3=β-lactamase inhibitor assay

Supplementary Material

Refer to Web version on PubMed Central for supplementary material.

Acknowledgements

We thank R. Ward, S. Levin, M. Elowitz, G. Bunin, A. Amir, S. Kryazhimskiy, Y. Gerardin, J. Meyer, E. Bairey, H. Chung, and A. Palmer for critical feedback and discussions; M. Baym, M. Fischbach, M. Traxler, R. Chait, L. Stone and E. Gontag for strains. EDK acknowledges government support under and awarded by the Department of Defense, Office of Naval Research, National Defense Science and Engineering Graduate (NDSEG) Fellowship, 32 CFR 168a. JZ acknowledges support from Research Science Institute at MIT during the summer of 2011. KV acknowledges startup funds from University of Wisconsin-Madison. RK acknowledge the support of a James S. McDonnell Foundation 21st Century Science Initiative in Studying Complex Systems Research Award 220020169, National Institutes of Health Grant R01GM081617, European Research Council Seventh Framework Programme ERC Grant 281891, Israeli Centers of Research Excellence I-CORE Program ISF Grant No. 152/11.

References

1. Hutchinson GE. The paradox of the plankton. American Naturalist. 1961; 95:137–145.
2. May RM. Will a large complex system be stable? Nature. 1972; 238:413–414. [PubMed: 4559589]
3. Levin SA. Dispersion and population interactions. American Naturalist. 1974:207–228.
4. Armstrong RA, McGehee R. Competitive Exclusion. The American Naturalist. 1980; 115
5. Levin SA. Community Equilibria and Stability, and an Extension of the Competitive Exclusion Principle. The American Naturalist. 1970; 104
6. Stewart FM, Levin BR. Partitioning of Resources and the Outcome of Interspecific Competition: A Model and Some General Considerations. The American Naturalist. 1973; 107:1–29.
7. Levin BR. Coexistence of two asexual strains on a single resource. Science. 1972; 175:1272–1274. [PubMed: 4551427]
8. Shoresh N, Hegreness M, Kishony R. Evolution exacerbates the paradox of the plankton. Proceedings of the National Academy of Sciences. 2008; 105:12365–12369.
9. Durrett R, Levin S. Spatial aspects of interspecific competition. Theor Popul Biol. 1998; 53:30–43. [PubMed: 9500909]
10. Czárán TL, Hoekstra RF, Pagie L. Chemical warfare between microbes promotes biodiversity. Proc Natl Acad Sci USA. 2002; 99:786–790. [PubMed: 11792831]
11. Kerr B, Riley MA, Feldman MW, Bohannan BJM. Local dispersal promotes biodiversity in a real-life game of rock-paper-scissors. Nature. 2002; 418:171–174. [PubMed: 12110887]
12. Reichenbach T, Mobilia M, Frey E. Mobility promotes and jeopardizes biodiversity in rock–paper–scissors games. Nature. 2007; 448:1046–1049. [PubMed: 17728757]
13. Hibbing ME, Fuqua C, Parsek MR, Peterson SB. Bacterial competition: surviving and thriving in the microbial jungle. Nat Rev Micro. 2010; 8:15–25.
14. Chait R, Vetsigian K, Kishony R. What counters antibiotic resistance in nature? Nat Chem Biol. 2012; 8:2–5. [PubMed: 22173342]
15. Conlin PL, Chandler JR, Kerr B. Games of life and death: antibiotic resistance and production through the lens of evolutionary game theory. Curr Opin Microbiol. 2014; 21:35–44. [PubMed: 25271120]

16. Green J, Bohannan BJM. Spatial scaling of microbial biodiversity. Trends in Ecology & Evolution. 2006; 21:501–507. [PubMed: 16815589]
17. Vetsigian K, Jajoo R, Kishony R. Structure and evolution of Streptomyces interaction networks in soil and in silico. PLoS Biol. 2011; 9:e1001184. [PubMed: 22039352]
18. Cordero OX, et al. Ecological Populations of Bacteria Act as Socially Cohesive Units of Antibiotic Production and Resistance. Science. 2012; 337:1228–1231. [PubMed: 22955834]
19. Raynaud X, Nunan N. Spatial Ecology of Bacteria at the Microscale in Soil. PLoS ONE. 2014; 9:e87217. [PubMed: 24489873]
20. Perlin MH, et al. Protection of Salmonella by ampicillin-resistant Escherichia coli in the presence of otherwise lethal drug concentrations. Proceedings of the Royal Society B: Biological Sciences. 2009; 276:3759–3768. [PubMed: 19656787]
21. Wright GD. Bacterial resistance to antibiotics: enzymatic degradation and modification. Adv. Drug Deliv. Rev. 2005; 57:1451–1470. [PubMed: 15950313]
22. Wootton JT. Indirect effects in complex ecosystems: recent progress and future challenges. Journal of Sea Research. 2002:1–16.
23. Ohgushi, T.; Schmitz, O.; Holt, RD. Trait-Mediated Indirect Interactions. Cambridge University Press; 2012.
24. Bollenbach T, Quan S, Chait R, Kishony R. Nonoptimal Microbial Response to Antibiotics Underlies Suppressive Drug Interactions. Cell. 2009; 139:707–718. [PubMed: 19914165]
25. Dugatkin LA, Perlin M, Lucas JS, Atlas R. Group-beneficial traits, frequency-dependent selection and genotypic diversity: an antibiotic resistance paradigm. Proceedings of the Royal Society B: Biological Sciences. 2005; 272:79–83. [PubMed: 15875573]
26. Yurtsev EA, Chao HX, Datta MS, Artemova T, Gore J. Bacterial cheating drives the population dynamics of cooperative antibiotic resistance plasmids. Mol Syst Biol. 2013; 9
27. Lenski RE, Hattingh SE. Coexistence of two competitors on one resource and one inhibitor: a chemostat model based on bacteria and antibiotics. J Theor Biol. 1986; 122:83–93. [PubMed: 3796009]
28. Hsu SB, Waltman P. A survey of mathematical models of competition with an inhibitor. Mathematical Biosciences. 2004; 187:53–91. [PubMed: 14609636]
29. Levin SA, Segel LA, Adler FR. Diffuse coevolution in plant-herbivore communities. Theor Popul Biol. 1990; 37:171–191.
30. Großkopf T, Soyer OS. Synthetic microbial communities. Curr Opin Microbiol. 2014; 18:72–77. [PubMed: 24632350]
31. D'costa VM. Sampling the Antibiotic Resistome. Science. 2006; 311:374–377. [PubMed: 16424339]
32. Walsh F, Duffy B. The culturable soil antibiotic resistome: a community of multi-drug resistant bacteria. PLoS ONE. 2013; 8:e65567. [PubMed: 23776501]
33. Brook I. The role of beta-lactamase-producing-bacteria in mixed infections. BMC Infect Dis. 2009; 9:202. [PubMed: 20003454]
34. Shaw KJ, Rather PN, Hare RS, Miller GH. Molecular genetics of aminoglycoside resistance genes and familial relationships of the aminoglycoside-modifying enzymes. Microbiol Rev. 1993; 57:138–163. [PubMed: 8385262]
35. Wetzstein HG, Stadler M, Tichy HV, Dalhoff A, Karl W. Degradation of ciprofloxacin by basidiomycetes and identification of metabolites generated by the brown rot fungus Gloeophyllum striatum. Applied and Environmental Microbiology. 1999; 65:1556–1563. [PubMed: 10103250]
36. Livermore DM. beta-Lactamases in laboratory and clinical resistance. Clin. Microbiol. Rev. 1995; 8:557–584. [PubMed: 8665470]
37. Rafii F, Hansen EB. Isolation of nitrofurantoin-resistant mutants of nitroreductase-producing Clostridium sp. strains from the human intestinal tract. Antimicrob. Agents Chemother. 1998; 42:1121–1126. [PubMed: 9593138]
38. Hoshino Y, et al. Monooxygenation of rifampicin catalyzed by the rox gene product of Nocardia farcinica: structure elucidation, gene identification and role in drug resistance. J. Antibiot. 2010; 63:23–28. [PubMed: 19942945]

39. Chait R, Craney A, Kishony R. Antibiotic interactions that select against resistance. Nature. 2007; 446:668–671. [PubMed: 17410176]

40. Chait R, Shrestha S, Shah AK, Michel J-B, Kishony R. A differential drug screen for compounds that select against antibiotic resistance. PLoS ONE. 2010; 5:e15179. [PubMed: 21209699]

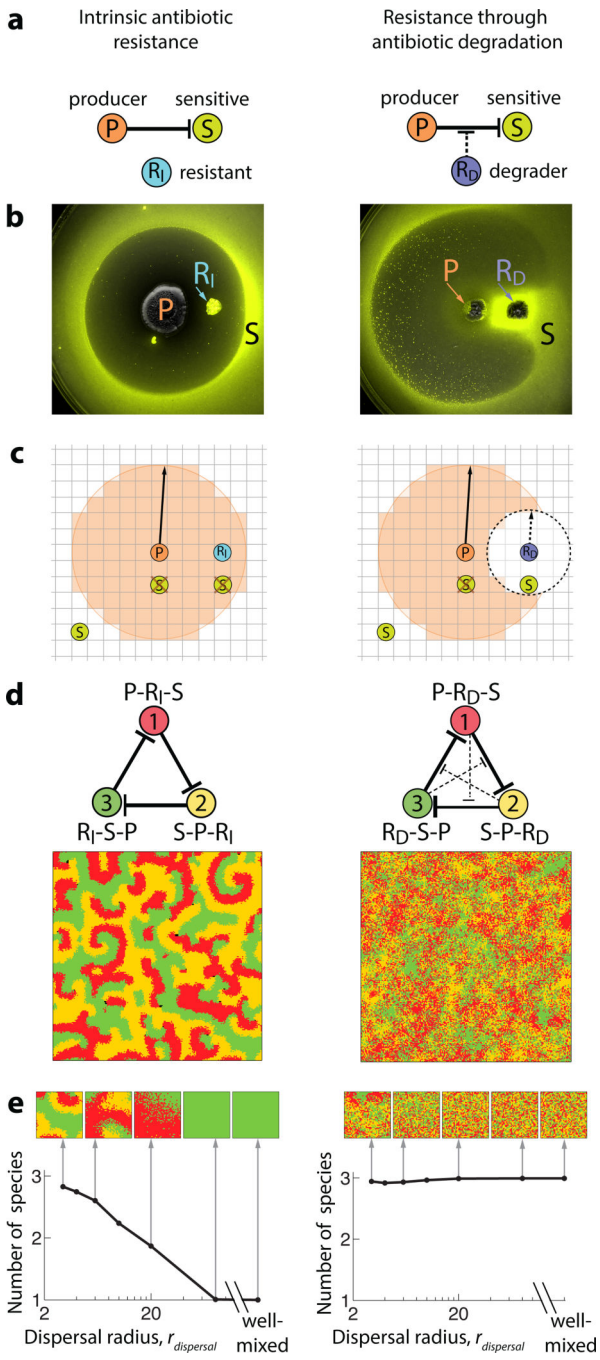

Figure 1. Replacing intrinsic antibiotic resistance with degradation-based resistance generates community robustness to species dispersal

a, Pairwise interactions among antibiotic producing (*P*), sensitive (*S*) and intrinsically resistant (R_I) species are compared to 3-way interactions where the sensitive species can be protected by an antibiotic degrading species (R_D). **b**, Images of a YFP-labeled probe *Escherichia coli* strain (*S*, yellow-green) growing in the presence of two *Streptomyces* colonies. The inhibition of the probe strain by a producer (dark area around *P*) is unaffected by an intrinsically resistant species (R_I, left), but is strongly attenuated around an antibiotic

degrading species (right, yellow-green halo around R_D colony). Images are representative of cases without and with 3-way interactions among 54 *Streptomyces* pairs tested (1 replica, Extended Data Fig. 1-2). **c**, Spatial inhibition-zone model: a producer (*P*) kills nearby species that are sensitive to its antibiotic (crossed out *S*), but does not affect resistant species (R_I, R_D). Sensitive species are protected by degrader species (right, *S* within dashed circle around R_D). Surviving species then replicate and disperse over distance $r_{dispersal}$. **d**, Snapshots of spatial simulations for cyclical 3-species 3-antibiotic interaction networks (labels indicate species phenotypes for each antibiotic). **e**, Intrinsically resistant communities collapse with increased dispersal (left), while communities with antibiotic degradation are robust to any level of dispersal (right). Insets show typical subregion snapshots. Number of species is based on average Shannon diversity of subregions (Methods).

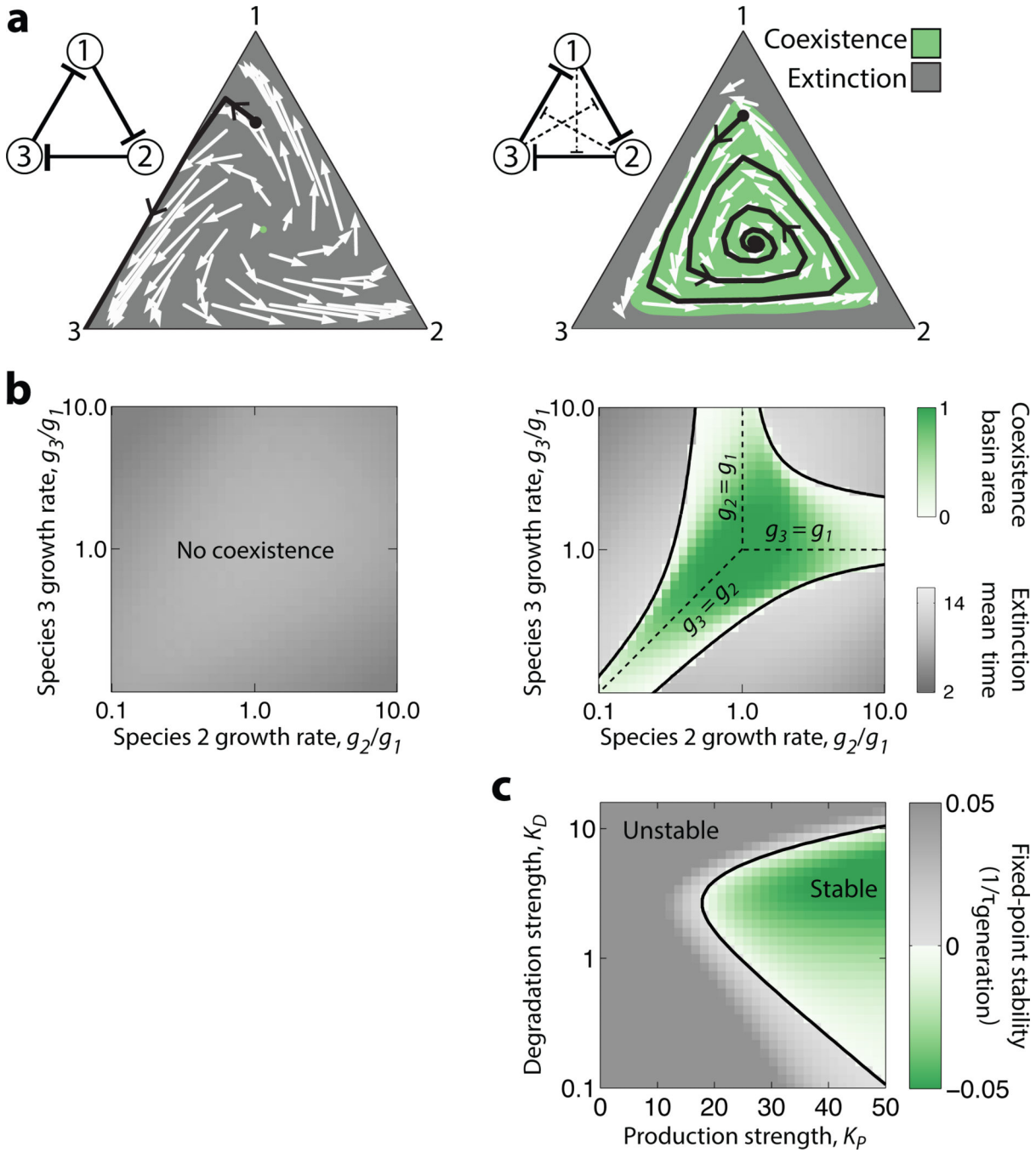

Figure 2. Strong antibiotic production with intermediate levels of degradation leads to stable communities robust to initial conditions and substantial differences in species growth rates

a, Communities with intrinsic resistance diverge from an unstable fixed point (green dot, left), while communities with antibiotic degradation converge toward a stable fixed point within a large basin of attraction (green area, right). Shown in trilinear coordinates are abundance changes per generation (white arrows) and example trajectories (black) for species with inherent growth rates: $g_1 < g_2 < g_3$. **b**, Communities with degradation remain stable even for large differences in inherent species growth rates (right), while communities

with intrinsic resistance are always unstable (left). **c**, Maximal community stability occurs at high levels of antibiotic production (K_P) and intermediate levels of degradation (K_D). Shading shows rate of exponential convergence (green) or escape (grey) from the fixed point. Black lines in panels **b-c** show the stability region boundary based on linear stability analysis (Methods).

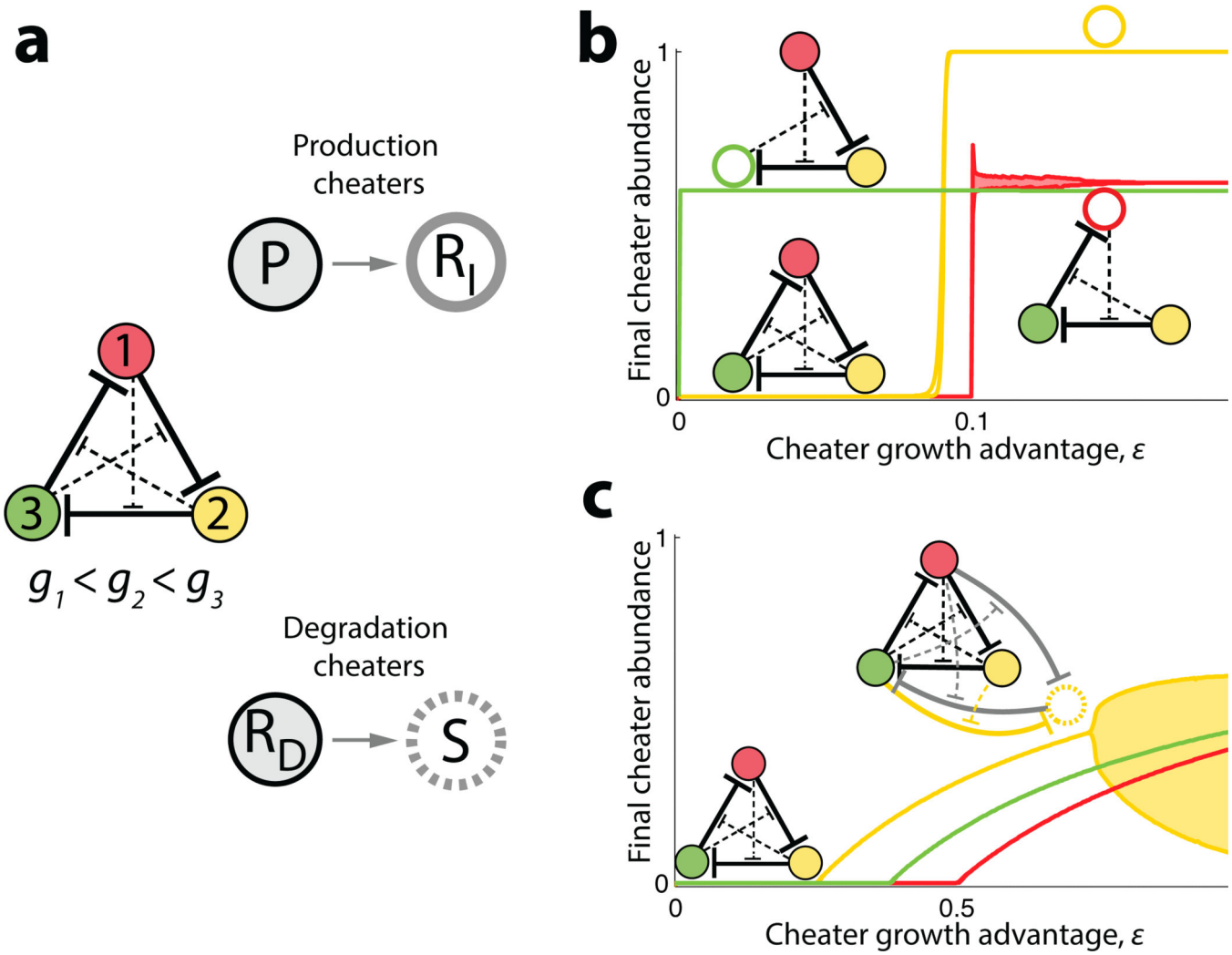

Figure 3. Communities are robust to invasion by cheaters that cease antibiotic production or degradation

a, Production or degradation cheaters (open circles with solid or dashed lines, respectively) are introduced at low abundance into a stable 3-species community (filled colored circles). **b**, When cheater growth advantage ε is small, only the production cheater of the fastest growing species can invade (species 3, green). This cheater replaces its parent, forming a new stable community, which is in turn robust to further invasions. The other two production cheaters can invade only when ε is large enough, taking over the community (yellow) or replacing their parent in a stable community (red). **c**, Degradation cheaters cannot invade the community at low ε, whereas at high enough ε they invade but do not replace their parents, rather generating a stable 4-species community. A 4-species interaction network is shown for the species 2 degradation cheater: gray interactions are inherited from the parent species; yellow interactions are specific to the cheater. Shaded areas span lower/upper bounds when the community exhibits sustained oscillations.

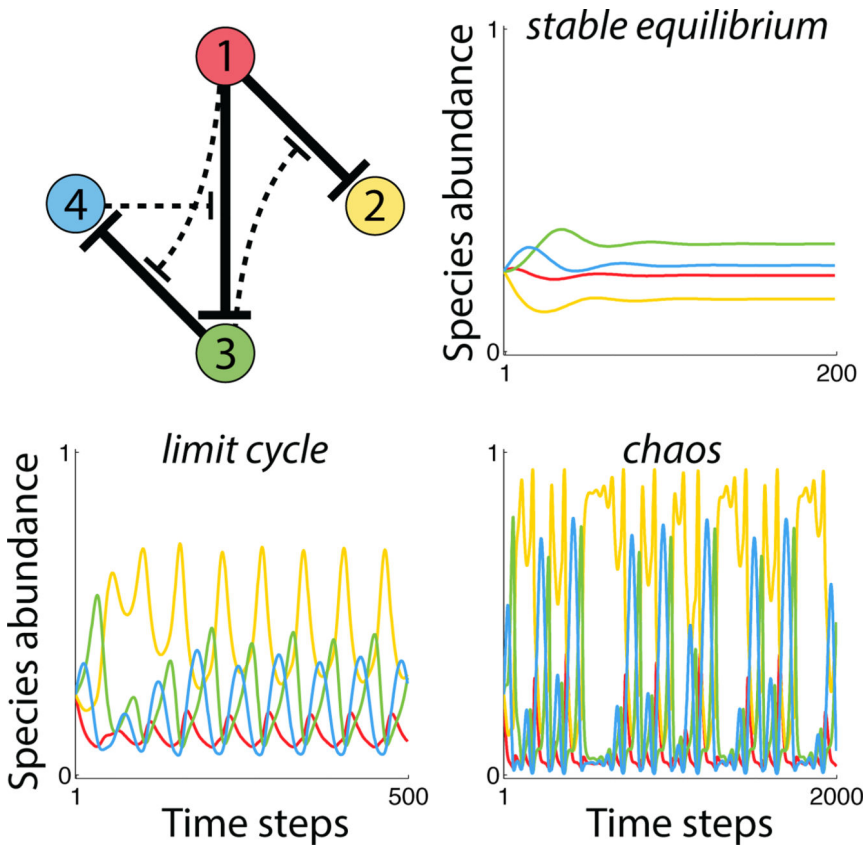

Figure 4. Complex interaction networks support coexistence through diverse dynamical behaviors

An example of a stable network with 4 species interacting through production and degradation of three antibiotics. Depending on the strengths of antibiotic production and degradation, this community can coexist through stable equilibrium, limit cycles or chaos (Methods). Line colors indicate species identity.